g6TiSCH: Generalized 6TiSCH for Agile Multi-PHY Wireless Networking

Mina Rady, Quentin Lampin, Dominique Barthel, Thomas Watteyne

IEEE Access
Multidisciplinary ⋮ Rapid Review ⋮ Open Access Journal

Received May 21, 2021, accepted May 26, 2021, date of publication June 3, 2021, date of current version June 17, 2021.

Digital Object Identifier 10.1109/ACCESS.2021.3085967

g6TiSCH: Generalized 6TiSCH for Agile Multi-PHY Wireless Networking

MINA RADY[1,2], QUENTIN LAMPIN[1], DOMINIQUE BARTHEL[1], AND THOMAS WATTEYNE[2], (Senior Member, IEEE)

[1]Orange Labs, 38243 Meylan, France
[2]EVA Team, Inria, 75012 Paris, France

Corresponding author: Mina Rady (mina1.rady@orange.com)

This work was supported in part by the French Agence Nationale de la Recherche under Contract CIFRE 2019/0605.

ABSTRACT Wireless networks traditionally use a single physical layer for communication: some use high bit-rate short-range radios, others low bit-rate long-range radios. This article introduces g6TiSCH, a generalization of the standards-based IETF 6TiSCH protocol stack. g6TiSCH allows nodes equipped with multiple radios to dynamically switch between them on a link-by-link basis, as a function of link-quality. This approach results in a dynamic trade-off between latency and power consumption. We evaluate the performance of the approach experimentally on an indoor office testbed of 36 OpenMote B boards. Each OpenMote B can communicate using FSK 868 MHz, O-QPSK 2.4 GHz or OFDM 868 MHz, a combination of long-range and short-range physical layers. We measure network formation time, end-to-end reliability, end-to-end latency, and battery lifetime. We compare the performance of g6TiSCH against that of a traditional 6TiSCH stack running on each of the three physical layers. Results show that g6TiSCH yields lower latency and network formation time than any of the individual PHYs, while maintaining a similar battery lifetime.

INDEX TERMS Agile networking, IoT, 6TiSCH, Industrial IoT.

I. INTRODUCTION

Applications of wireless connectivity span a growing number of use-cases. Within few decades, these use-cases spanned areas such as environmental monitoring [1], smart building [2], [3], precision agriculture [4], automated meter reading [5], indoor localization [6], micro-robot connectivity [7], smart grid management [8] and predictive maintenance [9]. Each application poses its own requirements for the quality of service expected from the network. Average current draw is often a key performance factor as devices are often battery powered and deployed in hard-to-reach areas. For some applications, the ability to communicate over a long distance is important as the network is deployed over a large area, or an area with poor propagation conditions. Other important network performance metrics include end-to-end reliability and latency.

This diversity in requirements means that different approaches are possible. Short-range radios generally lead to an improved battery lifetime and can offer satisfying coverage for some applications involving few nodes within a building-floor [2], [3], a peach orchard [4], [6], or a few single-chip micro-motes [7]. Long-range radios can offer the necessary coverage for deployments spanning multiple km^2 such as a large factory [9] or a power grid [8], at an acceptable compromise in battery lifetime [10]. In the rest of this article, we use the term "PHY" to refer to a combination of modulation, bit-rate, and frequency band.

Accordingly, advances have been accomplished in the manufacturing of radio chips and Systems-on-Chip (SoCs), leading to lower costs with more features and PHY capabilities. For example, the CC2538 SoC by Texas Instruments implements the IEEE802.15.4 PHY in the 2.4 GHz band which serves a sector of the short-range PHY market [11]. The Nordic Semiconductor nRF52840 SoC offers support of multiple protocol stacks for short-range PHYs such as IEEE802.15.4 and Bluetooth Low Energy (BLE) [12], both at 2.4 GHz. The AT86RF215 by Atmel implements the full range of modulations under the IEEE802.15.4g amendment [13] in both the 2.4 GHz band and the sub-GHz band.

The associate editor coordinating the review of this manuscript and approving it for publication was Bong Jun David Choi.

Its design allows switching between modulations on a frame-by-frame basis which enables it to serve both long-range and short-range applications [14].

A traditional approach followed by network solution architects is to compare different PHYs and choose the one most suitable for a given application. However, this approach leads to further constraints: if one PHY is used, the benefits of other PHYs are forfeited. If the application demands a change or a tuning (for example, a subset of nodes requires longer-range PHY), the entire network must be re-engineered to integrate a separate network using the new PHY running side-by-side (as discussed in Section II). This leads to an agility challenge as the network is becoming more complex to maintain and to improve.

The Internet Engineering Taskforce (IETF) is organized in Working Groups, some of which standardize IoT protocols. One of these Working Groups standardizes a set of standards for Industrial IoT applications, which require high reliability: the IPv6 over the Time Slotted Channel Hopping mode of IEEE802.15.4e (6TiSCH) Working Group. At the Medium Access Control (MAC) layer, 6TiSCH uses the IEEE802.15.4e TSCH mode, which is also at the root of industrial wireless protocols such as WirelessHART and ISA100.11a. In TSCH, a node cuts time into slots. A communication schedule orchestrates all communication, indicating to each node what to do in each slot: transmit, receive or sleep. Combined with channel hopping, this leads to high end-to-end reliability, and can be used in networks with a high traffic rate. At the PHY layer, 6TiSCH only supports a single PHY for the entire network. Currently, the chosen PHY for the standard stack is IEEE802.15.4 at 2.4 GHz.

Our vision is to have an agile wireless network where different PHYs can co-exist in the same network. This allows nodes to chose the most appropriate PHY on a frame-by-frame basis. A node dynamically switches between PHYs: a short-range PHY when the next hop is close by, a long-range PHY when the next hop is far away. On top of saving energy, this approach allows increasing robustness as some long-range PHYs are more robust against path-loss (e.g., FSK 868 MHz [2]) while others are more robust against multi-path fading and channel selective interference (e.g., OFDM 868 MHz [1], [2], [15]). All motes are still part of the same network in spite of their diverse PHYs.

The main contribution of this paper is generalizing 6TiSCH to support a multi-PHY approach; we call this ''g6TiSCH''. In g6TiSCH, nodes dynamically switch between using low bit-rate and high bit-rate PHYs, based on the link quality to each neighbor. We implement g6TiSCH in OpenWSN,[1] the reference 6TiSCH open-source implementation [16]. In this implementation, we use three PHYs: FSK 868 MHz option 1 at 50 kbps (offering the lowest bit-rate), OFDM 868 MHz option 1 MCS 3 at 800 kbps (offering the highest bit-rate), and O-QPSK 2.4 GHz at 250 kbps as an intermediate option.

[1] As an online addition to this article, the source code is available under an open-source license at http://github.com/openwsn-berkeley/.

We experimentally compare the performance of g6TiSCH against the performance of the 6TiSCH architecture with each PHY individually (as previously studied [17]). The comparison is based on the Key Performance Indicators (KPIs) recommended in by Vucinic *et al.* [18]: network formation time, end-to-end latency, end-to-end reliability, and battery lifetime.

The remainder of this article is organized as follows. Section II provides an overview of the related work. Section III presents the problem statement and lists the contributions of this article. Section IV shows how the 6TiSCH stack is adapted to provide multi-PHY support. Section V introduces the experimental testbed we used and the methodology we followed to generate the KPIs. Section VI discusses experimental results. Finally, Section VII concludes this article.

II. RELATED WORK

This section surveys the work most related to this research. We group related work into four focus areas: evaluation of IEEE802.15.4g PHYs (Section II-A), multi-PHY integration (Section II-B), routing in multi-PHY networks (Section II-C), 6TiSCH performance evaluation with different PHYs (Section II-D).

A. EVALUATING IEEE802.15.4g RADIOS

Several studies examine the link performance of the different PHYs within the IEEE802.15.4g (2012) amendment for the IEEE802.15.4 (2003) standard. This amendment proposes 31 PHYs for Smart-metering Utility Network (SUN) applications. They are based on three families of modulations: Frequency Shift Keying (FSK), Offset Quadrature Phase-Shift Keying (O-QPSK) and Orthogonal Frequency Division Multiplexing (OFDM). Data rates range from 25 kbps to 800 kbps. Two frequency bands are used: 2.4 GHz and sub-GHz.

Muñoz *et al.* [1] run an exhaustive experimental campaign using all 31 PHYs in four relevant outdoor settings: line of sight, smart agriculture, urban canyon, smart metering. Range-test performance is evaluated in terms of PDR, throughput, and current draw. Authors observe the longer range of FSK and O-QPSK in the sub-GHz band compared to OFDM options, enabled by their higher receiver sensitivity.

The same authors conduct a second experimental campaign in order to compare the performance of IEEE802.15.4 O-QPSK 2.4 GHz at 250 kbps, and IEEE802.15.4g OFDM [2]. They demonstrate the higher robustness of OFDM, even as it operates at a higher bit rate (800 kbps). They show that, although a radio draws less current when running O-QPSK 2.4 GHz, using OFDM 868 MHz leads to an overall lower power budget as transmission happens much faster.

Kojima *et al.* [15] measure the influence of interference between MR-FSK mode 2 and MR-OFDM option 4 MCS 3. They use the IEEE802.15.4e MAC with support for multi-hop forwarding on top of each PHY layer, and quantify the

influence of the interference between two networks, each running one of the PHYs. The authors show that OFDM performs better than FSK in the presence of narrow band interference since the former uses multiple sub-carriers.

These papers provide interesting results on the link-level performance of different PHYs. This paper goes one step further by integrating hybrid PHYs in a full protocol stack and evaluating the end-to-end performance of the hybrid stack.

B. MULTI-PHY INTEGRATION

Some recent proposals use hybrid PHYs in an integrated network. The study by Brachmann *et al.* [19] demonstrate enabling multi-PHY capability in the 6TiSCH stack. The authors run link performance testing campaigns using multiple PHYs: 2-GFSK (at 1.2 kbps, 8 kbps, 50 kbps, 250 kbps), 4-GFSK (at 1000 kbps), O-QPSK 2.4 GHz (at 250 kbps). Authors choose two PHYs in the sub-GHz band for integration in the 6TiSCH MAC layer: 2-GFSK at 1.2 kbps for transmitting Enhanced Beacons (EB), 4-GFSK at 1000 kbps for data traffic. The slot templates for the PHY layers are defined in accordance with the IEEE802.15.4 standard, and used in Contiki-NG. They demonstrate that the faster bit-rate of 4-GFSK at 1000 kbps for data packets reduces the collision probability and leads to less than 0.1% channel utilization despite the higher re-transmission rate. Furthermore, the slower bit-rate of 2-GFSK at 1.2 kbps leads to higher channel occupancy, at 2% duty cycle.

The proposal by Van Leemput *et al.* [20] is the state-of-the-art in multi-PHY integration in TSCH networking. The authors propose using slower PHYs for unicast links in case the Received Signal Strength Indicator (RSSI) is persistently below a certain threshold. PHY switching occurs at the MAC layer by continuously assessing the link's RSSI, using an Exponentially Moving Average filter. The timeslot is long enough for a single packet when using a low bit-rate radio, or multiple back-to-back packets when using a high bit-rate radio. The authors demonstrate a link's throughput can be increased by 153 % with only 84 % power consumption. This is achieved by using single acknowledgement for multiple packets in the same slot.

Garrido-Hidalgo *et al.* [21] develop a body-area network (BAN) using BLE mesh in the 2.4 GHz band. The mesh connects BLE wrist-bands worn by factory workers along with BLE-based machine sensors. The devices capture data relevant for safety in a real industrial setting. Collected data is forwarded to a BLE gateway which has a LoRaWAN interface that relays the data over long-range PHY in the sub-GHz band to a LoRaWAN gateway connected to the cloud.

These papers provide insightful performance evaluation of three kinds of multi-PHY networks. First, Brachmann *et al.* integrate two PHYs under one protocol stack; however, only one PHY is used as a default setting for data packets. Our proposed g6TiSCH architectures introduces a fully generalized stack where nodes can use hybrid PHYs for different neighbors for data transmission or reception and a node can switch its PHY dynamically depending on the neighbor. Second, the architecture proposed by Van Leemput *et al.* also integrates two sub-GHz PHYs under one protocol stack; however, the link switching mechanism occurs at the MAC layer. The authors show significant throughput improvement and energy savings using their multi-PHY architecture at the MAC layer. This confirms the intuition behind using multiple PHYs in the same TSCH-network. g6TiSCH goes one step further by allowing the integration of any number of (multi-band) PHYs. g6TiSCH also allows exposing the different costs associated with each PHY to the routing layer. It becomes aware of such costs and can improve the network energy footprint by selecting less costly PHYs when possible. This way, the routing layer cooperates with the lower layers. Furthermore, they demonstrate how the PHY-switching mechanism adapts the used PHY in case of switching to a PHY *of the same parent node.* g6TiSCH goes a step further by proposing a PHY-switching mechanism that is demonstrated in case of switching to a PHY of the same parent node or of a different parent node, since both cases are treated the same way. We further demonstrate the end-to-end performance of the resulting architecture for a holistic performance evaluation and we compare it to single-PHY architectures. Third, Garrido-Hidalgo *et al.* integrate two full stack networks side-by-side: LoRaWAN and BLE mesh to benefit from long-range and short-range PHYs. Since the g6TiSCH architecture proposed in this paper allows co-existence of multiple PHYs under one protocol stack, it allows less network management overhead and easier integration than multiple independent full-stacks.

C. ROUTING IN MULTI-PHY NETWORKS

Further studies address the theory and simulation of routing protocols on top of heterogeneous links. Lemercier *et al.* [22] propose enhancements to the IPv6 Routing Protocol for Low-Power and Lossy Networks (RPL) routing protocol to support hybrid PHYs: IEEE802.15.4 radio and Narrow Band Power Line Communication (PLC). The article proposes three suggested enhancements: Multiple RPL Instances Directed Acyclic Graph (DAG), parent-oriented DAG and radio interface-oriented DAG. The authors assume nodes with multiple interfaces: PLC and IEEE802.15.4. They run extensive simulations using the three routing solutions. Simulation results demonstrate that using hybrid interfaces offer improved network performance for all RPL enhancements chosen.

Al-Saadi *et al.* [23] propose a hybrid network architecture integrating Long Term Evolution (LTE) ''eNodeB'' base stations with a WiFi mesh based on an IEEE802.11 stack. The architecture enables relaying traffic among nodes with multiple interfaces: LTE, WiFi, Ethernet. This enables utilization of unlicensed band of WiFi to improve LTE coverage via WiFi mesh networks, without having to buy more of the licensed spectrum of LTE. The authors make use of the multi-rate feature of WiFi to combat interference and use a re-enforcement learning algorithm that determines for each node which technology to use for forwarding. They use

simulations to demonstrate that the overall network throughput is increased.

These papers introduce significant advances in theory of routing over hybrid networks to benefit from PHY diversity. First, Lemercier *et al.* consider a combination of wireless and wired links. The g6TiSCH architecture addresses the challenge of a fully wireless architecture which is more vulnerable to contention, fading, and interference. We demonstrate a real deployment including long-range PHYs with wire-like end-to-end reliability. Second, Al-Saadi *et al.* propose running full-stacks of WiFi and LTE side-by-side on relay nodes. This paper goes a step further by introducing a unified protocol stack and providing experimental evaluation of its performance.

D. 6TiSCH PERFORMANCE WITH DIFFERENT PHYs

The study in [17] evaluates the performance of the full 6TiSCH stack using different PHYs. The end-to-end performance of each network is evaluated experimentally. The study lays out a principle of ''no free lunch'' as it demonstrates that each PHY leads to enhanced performance of 6TiSCH in some aspects at the cost of lower performance in other aspects. For example, using FSK 868 MHz leads to shortest end-to-end latency but shortest battery lifetime, exactly opposite of O-QPSK 2.4 GHz. The study demonstrates a potential benefit from using all PHYs in one architecture so the network can combine their benefits, which serves as the foundation for this article.

Studies presented in this related work section provide insights on novel approaches for multi-PHY networking. This article introduces a generalized full protocol stack where nodes can use hybrid wireless PHYs for different neighbors. This builds upon [17] by integrating all three PHYs in one architecture. We demonstrate a real deployment with multi-PHY wireless networking with wire-like end-to-end reliability, with a mix of long-range and short-range radios.

III. PROBLEM STATEMENT AND CONTRIBUTIONS

As noted in the previous section, several studies have explored comparing and integrating multiple PHYs in hybrid architectures. These studies indicate the significance of hybrid networks. However, the challenge remains for a fully wireless, single-stack architecture that can accommodate a set of PHYs and yet offer wire-like reliability, especially for low-power and lossy applications.

The 6TiSCH protocol stack combines low-power operation and high reliability. It only uses one PHY, which is IEEE802.15.4 O-QPSK 2.4 GHz. Muñoz *et al.* have outlined the challenges and opportunities for a generalized 6TiSCH architecture [24]. One challenge is that the difference in energy consumption between the PHYs changes how the cost of communication to different neighbors is measured at the link-layer. This also affects how multi-hop paths are formed by the routing protocol. PHYs differ in their expected number of re-transmissions, resulting level of interference and resulting contention in shared cells (a cell is the combination of a location of a time-slot in the schedule and a frequency setting) [25]. Furthermore, previous experiments in [17] show system-level side-effects of each PHY. That is, a short-range PHY such as O-QPSK 2.4 GHz leads to a higher probability of packet queue overflow for increased re-transmissions and forwarding, which leads to packet drop. A long-range PHY such as FSK 868 MHz leads to a higher probability of neighbor table overflow due to an increased number of discovered neighbors, which leads to denial of service to possibly good neighbors.

This paper goes one step further by demonstrating a generalized 6TiSCH stack for multi-PHY wireless networking. The contributions of this paper are three-fold:

- We detail the minimal adaptations we had to do on some layers of the 6TiSCH protocol stack to support the g6TiCH architecture.
- We augment the OpenWSN reference implementation of 6TiSCH with g6TiSCH support, and compare its performance to single-PHY networks using O-QPSK 2.4 GHz, OFDM 868 MHz, and FSK 868 MHz.
- We evaluate end-to-end performance using industrial KPIs, and show how g6TiSCH provides a more balanced performance compared to single-PHY networks.

The following section gives an overview of 6TiSCH and how it is adapted for a generalized multi-PHY support in g6TiSCH.

IV. ADAPTING 6TiSCH FOR A GENERALIZED MULTI-PHY SUPPORT

Several articles shed light on 6TiSCH evolution and state of the art. Vilajosana *et al.* [26] provide a detailed tutorial on the stack of protocols adopted by the IETF 6TiSCH working group. For the purpose of this paper, we focus on the basic overview of the protocol stack for a reader without previous knowledge of 6TiSCH.

The main vision of 6TiSCH is to benefit from the industrial reliability of IEEE802.15.4e TSCH under a generic IP routing layer [27]. To achieve such integration, an adaptation layer called 6LoWPAN has been introduced to enable IP operation on a TSCH-based MAC layer. 6LoWPAN describes how neighbor advertisement and discovery should take place using the ''minimal'' shared cells as outlined in [28]. These advertisements are carried in 802.15.4 TSCH Enhanced Beacons (EBs) [29]. As neighbors are being discovered, the RPL routing algorithm chooses one or more neighbors to be routing parents, according to an objective function [30]–[32]. The objective function can consider one or more parameters for link cost estimations [32]. When a parent is selected, a node negotiates with its parent to add dedicated cells for uplink traffic using the 6TiSCH Operation Sublayer Protocol (6top) [33]. 6top negotiations occur via autonomous cells: each node allocates a default cell to receive negotiation requests, the index of this cell is calculated by a hashing function based on the slotframe length and the mote's MAC address [34]. After cells are allocated, the node broadcasts its routing information and the cost of the path between

TABLE 1. An outline of the relevant standards of the 6TiSCH protocol stack referenced in this paper.

Routing Layer (RPL)	RFC6550	2012	Main RPL Specification
	RFC6551	2012	Definitions for RPL Metrics
	RFC6552	2012	RPL default Objective Function Definition
6LoWPAN Adaptation Layer	RFC8505	2018	Describes neighbor discovery, registration, and managment policies
6TiSCH MAC Scheduling Layer	Minimal Scheduling Function draft	WIP	Describes the distributed schedule allocation
	Minimal security draft	WIP	6TiSCH Security and Constrained Join Protocol
	RFC8480	2018	6TiSCH Operation Sublayer Protocol (6top) describing how neighbors negotiate their links
	RFC8180	2017	Minimal 6TiSCH standard: detailing neighbor advertisement and discovery
	IEEE802.15.4e	2012	Standardized time-slotted channel hopping for medium access for deterministic IoT networks used in industrial applications
Physical Layer	IEEE802.15.4g	2015	An amendment to the IEEE802.15.4 standard, which introduces 31 PHYs for IoT networks in the 2.4 GHz band and the sub-GHz band
	IEEE802.15.4	2001	Standardized O-QPSK radio for IoT networks in the 2.4 GHz band

the node and the root (i.e. rank). These RPL broadcasts are called Destination-oriented directed acyclic graph Information Objects (DIOs). This information allows neighboring nodes to calculate the best route to use for their traffic.

In our generalized architecture, the following adaptations have been introduced to the 6iTSCH protocol stack:

- In Section IV-A, we show how TSCH is combined with Time-Slotted Physical-layer Hopping. This allows a mote to choose a different physical layer at each slot: radio channel, frequency band, radio modulation and the radio chip used (in case of multiple radio interfaces).
- In Section IV-B, we show how minimal cells are used to broadcast EBs and DIOs on each PHY. This enables nodes to synchronize and then discover neighbors on each PHY.
- In Section IV-C, we show how the objective function used by the routing algorithm is adapted to favor of parents with energy efficient PHYs. The 6top Protocol (6P) is then adapted so that nodes can determine the type of PHY they need in their requested cells. The longest range radio, FSK 868 MHz, is also used as a default for autonomous cells.

The remainder of this section will go over each adaptation in more detail.

A. TIME SLOTTED PHYSICAL-LAYER HOPPING

The IEEE802.15.4 (2015) standard defines the notion of a "PHY" as the combination of "the radio frequency (RF) transceiver and its low-level control mechanisms" (see [35], Section 5.6). It also defines the "channel" as the RF used by the transceiver for transmissions and receptions (Sections 10.1 and 11.3). The IEEE802.15.4e MAC layer of 6TiSCH uses channel hopping over 16 channels for O-QPSK 2.4 GHz.

In g6TiSCH, we introduce time-slotted PHY hopping for medium access: for a mote, time is divided into slots and in each time slot, the mote selects a specific PHY layer independent from the one used in the previous slot. The mote selects the most appropriate PHY at each slot depending on the negotiated links and protocol stack configuration. In our implementation, we use the OpenMote which features two radio chips: Atmel AT86RF215 which implements FSK 868 MHz and OFDM 868 MHz in the sub-GHz band, Texas Instruments CC2538 which implements O-QPSK in the 2.4 GHz band. FSK 868 MHz offers the lowest bit-rate at 50 kbps, OFDM 868 MHz offers the highest bit-rate at 800 kbps, and O-QPSK 2.4 GHz offers an intermediate bit-rate at 250 kbps. Their physical properties are outlined in Table 2.

TABLE 2. Characteristics of the selected PHYs.

	FSK 868 MHz	OFDM 868 MHz	O-QPSK 2.4 GHz
Radio chip	AT86RF215	AT86RF215	CC2538
Data rate	50 kbps	800 kbps	250 kbps
Output power	+14.5 dBm	+10.0 dBm	+7.0 dBm
Sensitivity	-114 dBm	-104 dBm	-97 dBm
Link budget	128.5 dB	114.0 dB	104.0 dB
Channel Spacing	0.2 MHz	1.2 MHz	2 MHz
Available Channels*	64	5	16

(*) The number of channels varies by regional regulations of each band. We consider the European 863-870 MHz band. A full list of available license-free bands is provided in the IEEE 802.15.4g amendment [13].

To use a different PHY at each slot, we extend the OpenWSN implementation with the `openradio` extension that allows a generic interface to the drivers of different chips from the MAC layer, as described in [17]. A distinct time-slot template is designed for each PHY. The concept of "time slot template" refers to the timings associated with each state of the IEEE802.15.4e state machine. These timings are affected by several factors, including the communication overhead for the Serial Peripheral Interface (SPI) which is the connection between the micro-controller and the radio chip, as well as the PHY bitrate. The timings are defined in Table 3 in the appendix, and are divided in two categories: *1)* board-specific timings, which depend on the performance of the firmware and the microcontroller and *2)* radio-specific timings, which depend on the performance of the specific radio chips used.

They are used to configure the state machine, which controls when a node switches state.

These timings are tuned with a logic analyzer; resulting templates are depicted in Fig. 1. We use a 40 ms timeslot duration in all cases to accommodate for the lowest bit-rate PHY, FSK 868 MHz. This decision is to allow for comparison with the results from the previous research in [17].

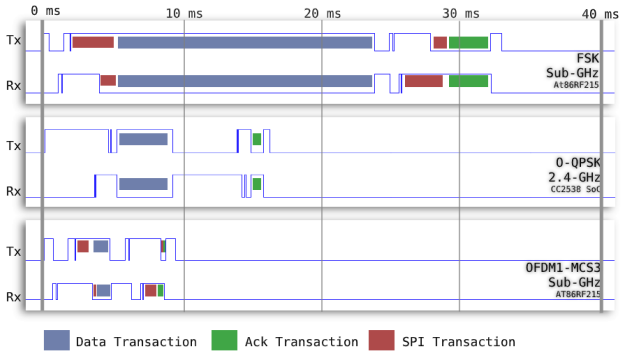

FIGURE 1. Timeslot templates for the three PHYs, for a 100 B data payload with acknowledgement. Red markers highlight when SPI transactions between the micro-controller and the AT86RF215 take place. We use a 40 ms timeslot duration for all the PHYs in both multi-PHY and single-PHY architectures (source: [17]).

B. GENERALIZED NEIGHBOR DISCOVERY AND NETWORK JOIN

In a traditional 6TiSCH network, when a new node is switched on, it keeps its radio on in receive mode, on the O-QPSK 2.4 GHz PHY. The radio slowly switches from channel to channel "scanning" the medium until it receives an EB broadcast from a synchronized node [29]. All synchronized motes transmit an EB with a given probability in the minimal shared cell. The EB contains details on the source mote, in addition to the specification of the slot-frame and the offset(s) of minimal cells that are used for EB broadcasts [28]. Once the new mote receives an EB, it synchronizes to the common slotframe shared by the network and starts aggressively duty-cycling its radio for energy-saving. The node keeps listening on minimal cells for more neighbors and then chooses one neighbor as a proxy for joining the network. It establishes a secure join procedure using Constrained Join Protocol [36] with the proxy mote using its autonomous cell.

In this g6TiSCH amendment, a minimal cell is allocated for *each* PHY for EB transmission. In this architecture, unsynchronized motes need to know which cells to use for EB broadcast and which PHY to use in each cell. To address this, we use the most significant byte in the `linkOptions` field to determine the PHY used for each minimal cell (Appendix A.1 in [28]). This way, when an unsynchronized mote processes an EB, it populates its schedule accordingly. As demonstrated in the sequence diagram in Fig. 2, the root transmits EBs on the 3 minimal cells. Mote *B* uses FSK 868 MHz for medium scanning since previous experiments in [17], [19] show that it leads to fastest

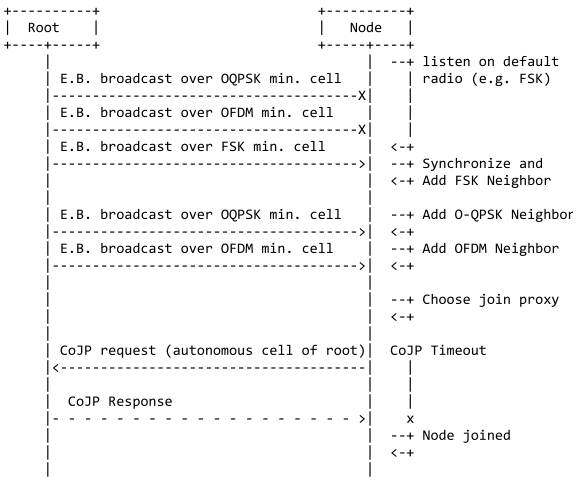

FIGURE 2. Neighbor discovery is adapted to listen on different PHYs for new neighbors. Use of hybrid PHYs on minimal cells enable faster neighbor discovery and Constrained Join Protocol handshake. Adapted from IETF draft [36].

synchronization (thanks to its longest range). Fast synchronization is important because it allows the mote to turn its radio off and save energy. When new mote *B* receives the EB transmitted from the root on the FSK 868 MHz minimal cell, it synchronizes to the network and registers the root in its neighbor table.

Other approaches could be used for neighbor discovery; for example, only one minimal cell can be allocated using the longest range PHY (e.g., FSK 868 MHz). This may lead to saving the energy for the two extra minimal cells. The benefit of using one minimal cell for each PHY is its simplicity as motes do not have to agree on a pre-specified PHY to synchronize into the network. Furthermore, increased contention is expected on the sub-GHz band because of its long range and on the 2.4 GHz band due to common Wi-Fi interference. Therefore, combining both bands improves discovery performance.

Then node *B* starts the neighbor discovery as it begins scanning the medium on the *minimal cell of each PHY* for more EBs from the neighboring PHYs. The use of multiple minimal cells allows the mote to discover available neighbors on each PHY. In this adaptation, PHYs of a neighboring mote are considered as different neighbors. In classical 6TiSCH, the minimal cells are used in either transmit or receive modes; that is, in case there are no packets queued for transmission, the mote goes to receive mode *by default*. Since g6TiSCH uses n times more PHYs than classical 6TiSCH, it also uses n times more minimal cells for neighbor discovery. This can cause it to consume, roughly, n times more power for broadcast cells. One way to mitigate this is as follows. In case there are no packets queued for transmission, each cell goes to receive mode with a given probability; otherwise, the PHY remains powered off for energy saving. We use $P_{rx} = \frac{1}{n}$, where P_{rx} is the probability to go in receive mode. This allows the mote to balance the energy spent in listening according

TABLE 3. Definition of timing variables that compose an IEEE 802.15.4e time-slot template.

Radio-specific variables	
TsTxOffset	The time between slot start and data transmission
TsLongGT	The maximum duration for radio to listen for the beginning of data packet
TsTxAckDelay	The time between packet reception and acknowledgment start of transmission
TsShortGT	The maximum duration for radio to listen for the beginning of acknowledgment packet
wdRadioTx	The maximum time for a radio chip to start frame transmission
wdDataDuration	The maximum time to complete a transmission of a data frame
wdAckDuration	The maximum time to complete a transmission of an acknowledgment frame
Board-specific variables	
maxTxDataPrepare	The maximum time to retrieve and prepare a data frame on transmitter side.
maxRxAckPrepare	The maximum time to retrieve and prepare an acknowledgement frame on receiver side.
maxRxDataPrepare	The maximum time to prepare for data frame reception on receiver side.
maxTxAckPrepare	The maximum time to prepare for acknowledgement frame reception on transmitter side.
delayTx	The expected delay between issuing a transmit command by the micro-controller and its execution on the radio-chip
delayRx	The expected delay between issuing a receive command by the micro-controller and its execution on the radio-chip

to the number of used PHYs. For example, a network that uses three PHYs would consume approximately 200% more power in minimal cells than a single-PHY network if the radio were never switched off in any of these cells. So, in a configuration with three PHYs, we use $P_{rx} = \frac{1}{3}$. Therefore, if there are no packets queued for transmission, the radio will turn on for reception in all cells approximately 100% instead of 300% of the time compared to single-PHY network. This way, the multi-PHY network will remain approximately at the same power consumption at minimal cells as the single-PHY network.

Node *B* starts the procedure to join the network according to the join protocol [36]. The procedure identifies the proxy the neighbor with the best join priority (the closer to the root, the better). It then sends the join request on the autonomous cell of the proxy (e.g. the root in this case). In this g6TiSCH amendment, FSK 868 MHz is used for communication on autonomous cells since it is the most robust PHY. When the request is authenticated and acknowledged by the root, the join procedure is successful, and *B* can proceed with parent selection and cell negotiation.

We note that security is an integral part of the 6TiSCH framework as defined in IEEE 802.15.4e (Section 7) [29] and the IETF 6TiSCH Minimal Security draft [36]. All the security features 6TiSCH carry over to g6TiSCH, including packet encryption and secure join.

C. GENERALIZED PARENT SELECTION AND LINK NEGOTIATION

The IETF RPL-related standards define mechanisms for neighbor evaluation and parent selection [30], [32]. In the IPv6 RPL routing layer of 6TiSCH, a node selects a parent mote by evaluating the expected path cost through each neighbor to the root and it chooses the parent with the least expected path cost. The cost of a single link is estimated based on the expected transmission count (ETX) ratio as in (1), as shown at the bottom of the page, where: *numTx* is the number of transmissions on the link and *numAck* is the number of acknowledgments received. This full path cost through neighbor *i* to the root is evaluated by the objective function based on (2), as shown at the bottom of the page, (as defined in the 6TiSCH minimal configuration [28]), where: $Rank_i$ is the advertised rank of the neighbor, *minHopIncrease* is the minimal cost to use for a one hop link. For example, the root has a default rank of 256. If a mote has a link to the root with perfect ETX ratio of 1, the expected path cost is 512. After a parent is selected, the routing algorithm can later decide to change the parent to new neighbor *i* if the condition in (3), as shown at the bottom of the page, evaluates to *true*. The factor *P* is the parent switch threshold so that the mote does not change parent unless it expects significant improvement (i.e. hysteresis). This way, the network avoids too frequent parent changes, which would lead to instability. The recommended configuration for this

$$ETX_i = \frac{numTx_i}{numAck_i} \tag{1}$$

$$Cost(Neighbor_i) = Rank_i + ((3 \cdot ETX_i) - 2) \times minHopIncrease. \tag{2}$$

$$f(Parent, Neighbor_i) = \begin{cases} true, & \text{if } Cost(Parent) - Cost(Neighbor_i) \geq P \\ false, & \text{otherwise} \end{cases} \tag{3}$$

$$Cost(Neighbor_i) = Rank_i + ((3 \cdot ETX_i) - 2) \times minHopIncrease \times Factor(PHY_i). \tag{4}$$

$$E_{bit}(PHY_i) = \frac{((I^i_{tx} + I^i_{rx}) \cdot V^i_s)}{R^i_b} \tag{5}$$

TABLE 4. PHY layers energy per bit estimations. OFDM 868 MHz is the lowest energy footprint per bit transmission/reception followed by O-QPSK 2.4 GHz and FSK 868 MHz.

	FSK 868 MHz	OFDM 868 MHz	O-QPSK 2.4 GHz
Radio chip	AT86RF215	AT86RF215	CC2538
Data rate	50 kbps	800 kbps	250 kbps
I_{TX}	62 mA	62 mA	24 mA
I_{RX}	28 mA	28 mA	20 mA
Supply voltage	2.5 V	2.5 V	3.0 V
Energy per bit	9.00 μJ	0.28 μJ	0.53 μJ

threshold is $2 \times minHopIncrease$, as proposed in the minimal 6TiSCH configuration [28].

In g6TiSCH, a combination of neighbor IPv6 address and a PHY link is considered an independent neighbor. The use of multiple PHYs poses the need for a metric to evaluate and compare different PHYs. There can be different ways to build this metric; for example, based on power consumption, latency, or time-on-air. We use a simple configuration for the routing layer that is sufficient to demonstrate the advantage of the g6TiSCH architecture.

Therefore, for the purposes of the experiment, we choose to evaluate the different PHYs based on energy consumption in order to extend the battery lifetime as much as possible. The objective function is adapted as in Eq. (4), shown at the bottom of the previous page, to compute the link cost of a certain "neighbor" by giving weight to the expected energy per bit E_{bit} for the PHY of that neighbor. Therefore, in case neighboring links have similar ETX ratios, the mote would favor PHYs with lower E_{bit} for energy saving.

To determine the order of the PHYs, we estimate the E_{bit} for each PHY as a function of its power consumption for transmission and reception and its bit rate. The function is expressed in (5), as shown at the bottom of the previous page, where I^i_{tx} and I^i_{rx} are the current draw for transmission and reception for PHY_i, V^i_s is the voltage supply for the radio chip of PHY_i, and R^i_b is the bit rate. Table 4 shows the E_{bit} for each PHY. Therefore, the least power consuming PHY is OFDM 868 MHz, followed by O-QPSK 2.4 GHz and FSK 868 MHz. We assign $Factor(OFDM) = 1$, and $Factor(OQPSK) = 2$. However, we assign $Factor(FSK) = 5$ just to make the switch to an FSK 868 MHz PHY harder than the switch to O-QPSK 2.4 GHz PHY, to account for its energy hungry footprint. Future work can focus in more detail on how such factors can be derived in a generic manner.

After the objective function converges on a given combination of neighbor IPv6 and PHY setting, the node initiates the request to allocate cells with the selected parent. In the standard 6TiSCH stack, cells are identified by a combination of slot offset and channel offset. The Minimal Scheduling Function [34] initiates a 6top request for the parent to allocate a dedicated cell for uplink traffic [33]. This 6top request be sent within a maximum period from the moment the routing algorithm decides on switching parents (whether switching between different PHYs or completely different nodes). This maximum period is called the "housekeeping" period which is part of the current draft of the Minimal Scheduling Function. This way, the latency of the parent-switching is has an upper-bound duration for a more deterministic performance. When the parent approves the request, the cell is allocated on both motes.

In g6TiSCH, the definition of a cell is extended to include the used PHY as well. The 6top request to add cells is extended to define what type of PHY it needs for that cell. A sequence diagram of the transaction is outlined in Fig. 3. We use two unused bits of the `linkOptions` byte to encode the PHY type of the requested cell. When the parent acknowledges the request, the cells are added on both sides and the uplink negotiation is complete.

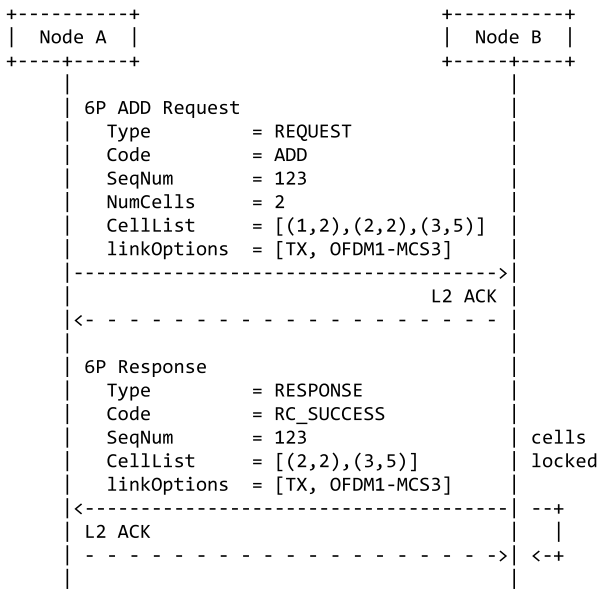

FIGURE 3. 6top protocol transaction to allocate a cell specifying its PHY layer radio setting. Adapted from IETF RFC8480 [33].

An example of a complete g6TiSCH slotframe is shown in Fig. 4 for a network of three motes: A is the root, B is a relay node, and C is a leaf node. Three minimal cells are allocated at the beginning of the slotframe, one for each PHY. EB and DIO broadcasts are transmitted within these slots for network synchronization and neighbor discovery.

Each mote allocates an autonomous cell using its FSK 868 MHz radio for 6top negotiation transactions. Mote B has up-link cells to A in slot 6 with OFDM 868 MHz PHY and Mote C also established an O-QPSK 2.4 GHz link to B in slot 5. Therefore, from a forwarding perspective, node B uses O-QPSK 2.4 GHz with its CC2538 radio chip to listen for data packets from C in slot 5 and channel 1. It then uses OFDM 868 MHz with its AT86RF215 radio chip to send up-link frames to A in slot 6 and channel 7.

V. EXPERIMENTAL SETUP AND METHODOLOGY

To examine the performance of the g6TiSCH architecture, we use the OpenTestbed [37] for experimental evaluation. Network performance is compared to 6TiSCH deployments with each PHY individually. This section gives an overview

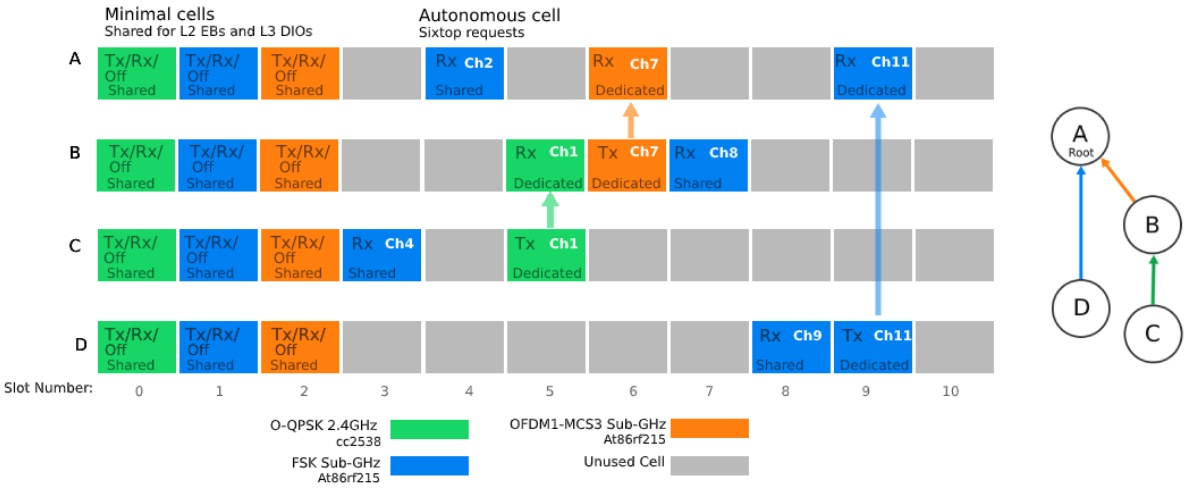

FIGURE 4. Example of a multi-PHY slot frame in the resulting generalized 6TiSCH architecture. A minimal cell for each PHY-layer enables discovery of different radios. FSK 868 MHz is used for autonomous cells. Node *C* allocates dedicated O-QPSK 2.4 GHz cells for its parent *B*. Node *B* allocates dedicated OFDM 868 MHz cells for its parent *A*. Node *C* allocates dedicated FSK 868 MHz cells for its parent *A*.

of the experimental setup (Section V-A) and the methodology for the performance evaluation for g6TiSCH and the single-PHY networks (Section V-B).

A. EXPERIMENTAL SETUP

We extended the OpenWSN 6TiSCH reference implementation with g6TiSCH. Before this update, the memory footprint of the full OpenWSN stack was 42 kB of flash. The size of the updated implementation is 79 kB, including the drivers for both the CC2538 and the AT86RF215 radio chips. This fits comfortably in modern micro-controllers, which typically feature 512 kB of flash memory. We use a slotframe duration of 41 slots, as previously used in [17] for comparison. The configuration of the protocol stack is detailed in Table 5.

TABLE 5. Parameters of the OpenWSN protocol stack.

Parameter	Value
Application traffic period	60 s
RPL DIO period	10 s
RPL DIO probability	10%
RPL DAO period	60 s
Packet queue size *	15
Slotframe length	41
Timeslot duration	40 ms
EB probability	10%
O-QPSK 2.4 GHz channels	16
FSK 868 MHz channels	16
OFDM 868 MHz channels	5
New neighbor RSSI threshold	−80 dBm
Max num. re-transmissions	15

* The buffer can hold up to 15 data packets (in addition to 5 reserved entries for network control packets).

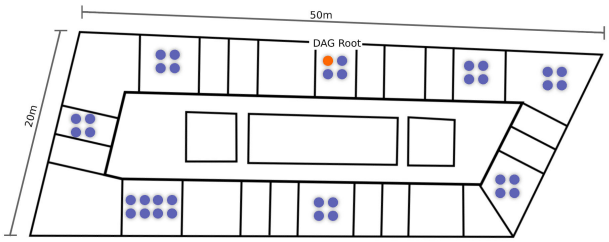

FIGURE 5. Locations of the 36 motes of the OpenTestbed across an office floor at Inria-Paris.(source: [37]).

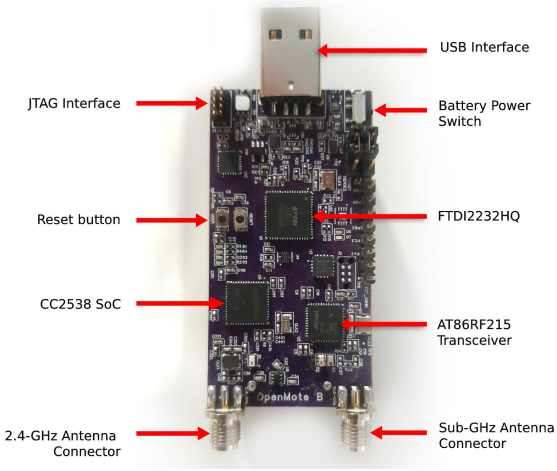

FIGURE 6. The OpenMote B board with multi-PHY support.

The OpenTestbed is deployed indoors in an office building at the Inria research center in Paris (floorplan on Fig. 5). The OpenTestbed is composed of 36 OpenMote B boards (shown in Fig. 6). The OpenMote B is a low-power wireless platform that features both a CC2538 SoC (a micro-controller and O-QPSK 2.4 GHz radio) and an AT86RF215 (an FSK 868 MHz and OFDM 868 MHz radio) [38]. It allows multi-band networking as it features two antennas: a 2.4 GHz

antenna connected to the CC2538 and a sub-GHz antenna connected to the AT86RF215. It is built around an ARM Cortex-M3 on the CC2538, with 32 kB of RAM and 512 kB of flash.

A total of 36 OpenMote B motes are deployed in clusters ranging between 4–8 motes, which is similar to a distribution of sensors around different machines in real industrial environment [9]. As described in [37], the OpenTestbed consists of Raspberry Pi single-board computers where each board has 4 OpenMote B boards attached to it (shown in Fig. 7). The Raspberry Pi computers are connected using 5 GHz Wi-Fi network to avoid interference with O-QPSK 2.4 GHz links. All these computers are connected to a central MQTT broker, allowing a user to remotely reprogrammed the OpenMote B boards, interact with their serial port, and reset the boards.

FIGURE 7. The OpenTestbox used for experimental evaluation in the Open Testbed (source: [37]).

B. METHODOLOGY

For experimentation, we use the same setup as in [17]. The network is run three times with each PHY individually. For short, the single PHY networks will be referred to by their PHY names hereafter (i.e., O-QPSK 2.4 GHz, FSK 868 MHz, and OFDM 868 MHz). It is then run a fourth time with the generalized multi-PHY architecture. This is to demonstrate that the generalized architecture is capable of providing a more balanced performance than each PHY individually. We ran that set of experiments at night for the building to be minimally occupied to increase repeatability between experiments. For each experiment, a mote placed in the middle of the floor is set as the DAG root (see Fig. 5) and the network is run for 90 mn.

To capture the network performance, we build an application that captures local measurements on each mote and transmits them via User Datagram Protocol (UDP) packets to the root. The following measurements are captured and sent every 60 s from each mote:

- a counter, that is used to detect loss of data packets.
- the time at which the data packet was created (expressed in Asynchronous Slot Number, ASN),
- the DAG rank of the sender,
- T_{on}: how long the sender's radio has been on since the previous data packet transmission,
- T_{TX}: how long the sender's radio has been on and transmitting since the previous data packet transmission,
- T_{on}^{FSK}, T_{on}^{OFDM}, and T_{on}^{OQPSK}: the breakdown of T_{on} for each PHY,
- T_{TX}^{FSK}, T_{TX}^{OFDM}, and T_{TX}^{OQPSK}: the breakdown of T_{TX} for each PHY,
- T_{total}: the amount of time since the previous data packet transmission,
- the maximum and minimum number of packets in the packet buffer since the previous packet.

After the experiment, we use the logged data to compute the following KPIs, as recommended by Vučinić *et al.* [18]:

- Network Formation Time: the time between the moment the root is switched on and the moment the root has received at least one application packet from *each* mote in the network.
- End-to-End Reliability: the portion of packets generated in the network that are received by the root.
- End-to-End latency: the time duration between generating the packet at the sender, and receiving it at the root.
- Radio duty cycle: the portion of the time a node's radio is on; a good indication for its power consumption and compliance to duty cycle regulations.

We are aware that end-to-end latency for OFDM 868 MHz and O-QPSK 2.4 GHz can be improved by using smaller slot durations (instead of the 40 ms timeslot). However, to maintain consistency across experiments, we choose to change one parameter only, the network PHY, in order to measure its impact on end-to-end KPIs. Therefore, we fix the slot-duration at 40 ms for all networks in order to isolate any possible effects of smaller slot durations (such as increased duty cycle). This way, we can ensure that our observations are strictly due to change of PHYs. We are also aware that use of different slot durations in the same slotframe for g6TiSCH can improve latency performance. However, we are interested in demonstrating the baseline performance of g6TiSCH in this study. Furthermore, we address this in a separate study since it touches on a separate research context of ''Schedule Compactness'' in TSCH networks.

We display the results in two forms:

- Time series: We plot the mean and the inter-quartile range of the KPI, with a sliding window of 3 mn and a time resolution of 1 s.
- Cumulative Distribution Function: We plot the cumulative distribution of data from packets received at steady state (starting 30 mn into the experiment), using 100 bins.

VI. EXPERIMENTAL RESULTS

This section details the findings from the experimental campaigns. We show the performance of the networks in terms of: Network formation time (Section VI-A), end-to-end latency (Section VI-B), end-to-end reliability (Section VI-C), and battery lifetime (Section VI-D).

A. NETWORK FORMATION

Network formation time is measured as the time between setting the DAG root until the time the root has received at least one packet from each mote. This duration of a *full join* process includes the time a mote synchronizes to the network, establishes a secure join hand-shake, and successfully negotiates a link to a parent (as outlined in Sections IV-B and IV-C). We assume a worst-case scenario as all motes are flashed at once and begin the network join procedure at the same time. This increases contention since neighbor discovery and link negotiations occur on shared cells. So this helps us observe the behavior of the network under stress.

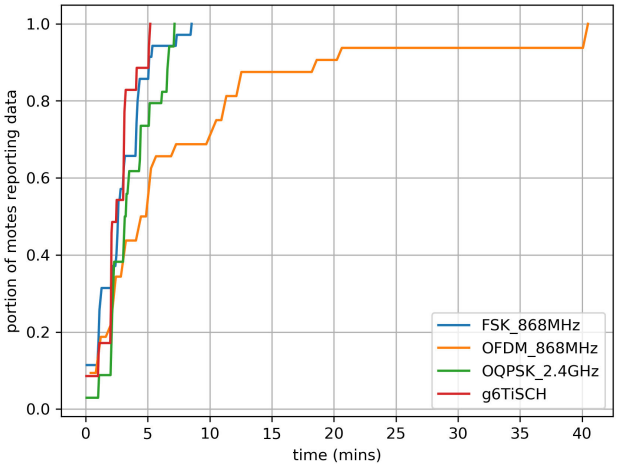

FIGURE 8. Dynamic selection among multiple radios allows a robust network formation, within the same order of magnitude as the long range FSK 868 MHz network.

We plot in Fig. 8 the cumulative density of the time-to-first-data-packet from each of the 36 motes in the network. For 90% of the motes, network formation time is 5, 5, 7, and 18 min for g6TiSCH, FSK 868 MHz, O-QPSK 2.4 GHz, and OFDM 868 MHz, respectively. Among the single PHY networks, the OFDM 868 MHz network is the slowest to form. This is because the low number of available channels (5) for OFDM 868 MHz Option 1 increases the probability of collision in shared cells, slowing down neighbor discovery. The g6TiSCH formation time is in the same order of magnitude as FSK 868 MHz and O-QPSK 2.4 GHz networks in spite of the larger number of available links. This is because the g6TiSCH network dynamically improves its selected PHYs, its formation time remains within the same efficiency.

This can be observed in Fig. 9, which shows the number of PHYs selected for routing as the g6TiSCH network is forming. The multi-PHY neighbor discovery enables the network to combine the advantages of each PHY. On minimal cells of long-range PHYs such as FSK 868 MHz, a mote can hear a larger portion of the network with an increased risk of contention. On minimal cells of short-range PHYs such as O-QPSK 2.4 GHz, a mote can hear a smaller portion of the network with less risk of contention. Therefore, this leads to an overall robust network formation.

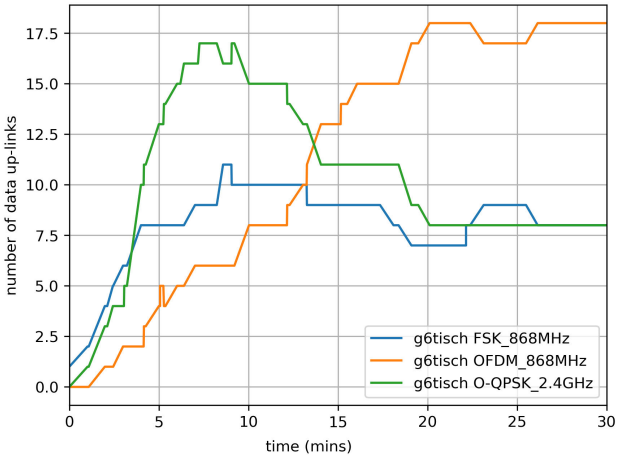

FIGURE 9. As the g6TiSCH data collection tree is forming, it routes up-link traffic over diverse PHYs.

B. END-TO-END LATENCY

The end-to-end latency is calculated based on the difference between the ASN when the UDP packet is generated and the ASN when it arrives at the root. It is affected by several factors including the number of hops between the mote and the root and the number of re-transmissions at each hop.

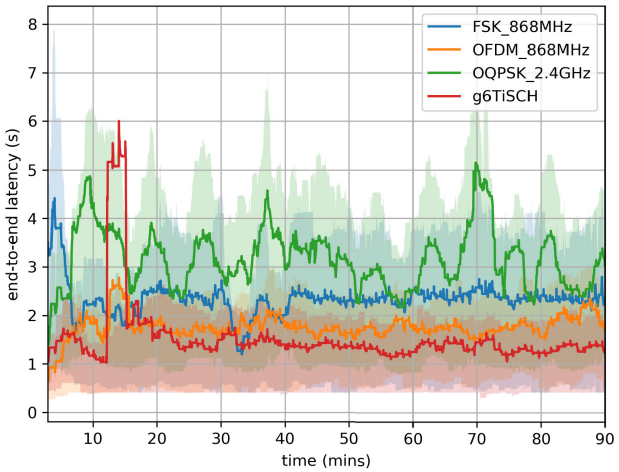

FIGURE 10. Using multiple radios at the same time yields lower end-to-end latency than using a single radio.

We show in Fig. 10 a time-domain plot of the end-to-end latency in the network. The cumulative density of all the packets, during the steady state phase, is shown in Fig. 11. The longer range of OFDM 868 MHz and FSK 868 MHz (due to the sub-GHz band) leads to lower latency because of decreased re-transmissions and decreased number of hops. This is because motes are able to reach closer to the root thanks to the low ETX.

The g6TiSCH architecture exhibits a latency improved over that of each single-PHY network, since the best PHY is selected at each hop. Interestingly, it even demonstrates better

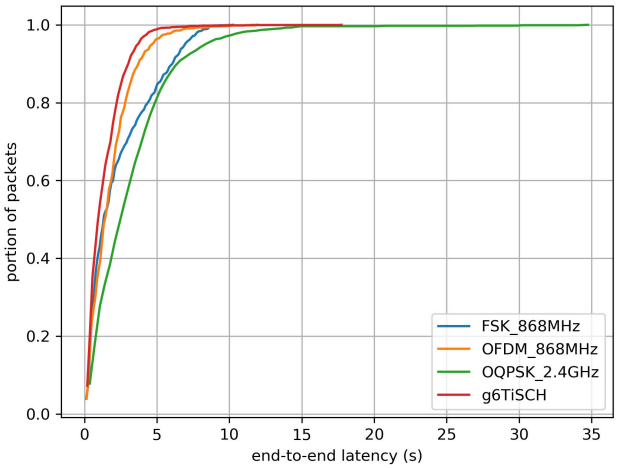

FIGURE 11. Cumulative distribution function of end-to-end latency, at steady state.

latency than the FSK 868 MHz network. This is because the routing layer favors a parent switch only if the rank difference is more than $2 \cdot minHopIncrease$ as expressed in Eq. 3, which is equivalent to two hops with perfect links. Therefore, if a mote is two hops away from the root, still it will not change to the root since the cost improvement is not high enough to motivate the change of parents. However, the $Factor(PHY_i)$ coefficient in the g6TiSCH objective function in Eq. 4 increases the cost of FSK 868 MHz link significantly, which gives more incentive to find better paths when possible, effectively leading to lower latency.

TABLE 6. End-to-end packet delivery ratio (PDR) statistics over all motes in the network, computed over the last 30 mn of the experiments.

	Min	Average	Median	Max	StDev
FSK 868 MHz	100.0%	100.0%	100.0%	100.0%	0.0%
OFDM 868 MHz	100.0%	100.0%	100.0%	100.0%	0.0%
O-QPSK 2.4 GHz	96.7%	99.7%	100.0%	100.0%	0.96%
g6TiSCH	100.0%	100.0%	100.0%	100.0%	0.0%

C. END-TO-END RELIABILITY

End-to-end reliability is measured using the packet counter in the UDP packet to identify lost packets. End-to-end PDR is the ratio of received packets to total packets sent from a mote. Table 6 shows a statistical summary for the PDR for all motes in the last 30 mn for each network. We note that the FSK 868 MHz network outperforms O-QPSK 2.4 GHz, which is consistent with the previous observation in [17]. g6TiSCH offers 100% reliability, the same as FSK 868 MHz, even though only 20% of the links used for routing use FSK 868 MHz (in steady state). The remaining links are 51% OFDM 868 MHz and 29% O-QPSK 2.4 GHz.

Packet loss can occur from packets being dropped because of buffer overflow. We show in Fig. 12 the maximum buffer size captured in the network. Both g6TiSCH and FSK 868 MHz show lower memory footprint than O-QPSK 2.4 GHz after 30 mn into the experiment. This is because of decreased re-transmissions and forwarding as explained in Section VI-B.

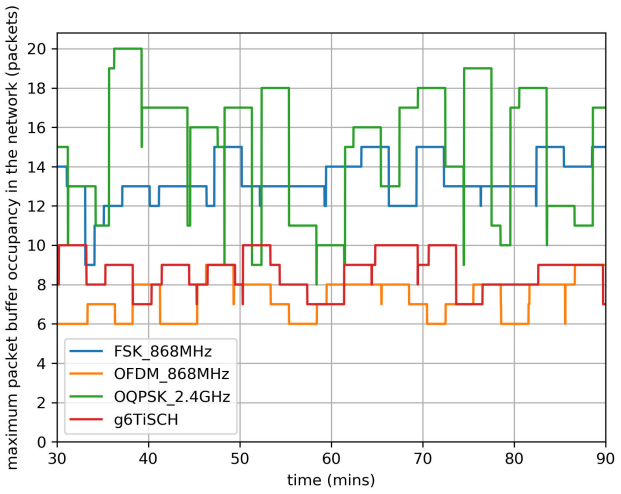

FIGURE 12. Improved overall link quality in g6TiSCH leads to efficient buffer usage due to less re-transmissions and forwarding. Packet buffer is efficiently used and packets are not dropped due to buffer overflow.

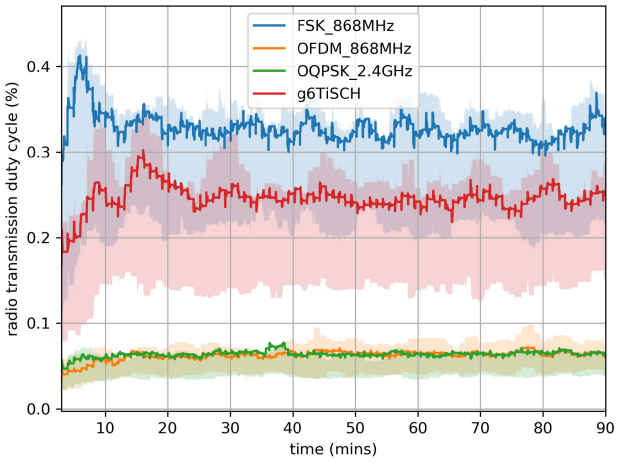

FIGURE 13. Diversity of radios allows overall lower radio duty cycle compared to a pure long range FSK 868 MHz network.

This demonstrates an advantage of the generalized architecture: it achieves reliability comparable to that of a full FSK 868 MHz network, yet with only 20% of FSK 868 MHz links.

D. BATTERY LIFETIME

The battery lifetime is estimated based on the measured radio duty cycle during the experiment. We measure the duration the radio spends transmitting and the total duration the radio is on (including the time the radio spends in receive mode). While this is not a precise predictor of the battery lifetime, it is an indicator of the order of magnitude of lifetime for each network. Therefore it is sufficient for the purpose of comparing the networks. Fig. 13 shows the evolution of the transmit duty cycle in the network over the experiment duration. g6TiSCH shows an overall lower radio duty cycle than FSK by nearly 30%. This is attributed to it using OFDM 868 MHz and O-QPSK 2.4 GHz extensively, benefiting from their higher bit-rates.

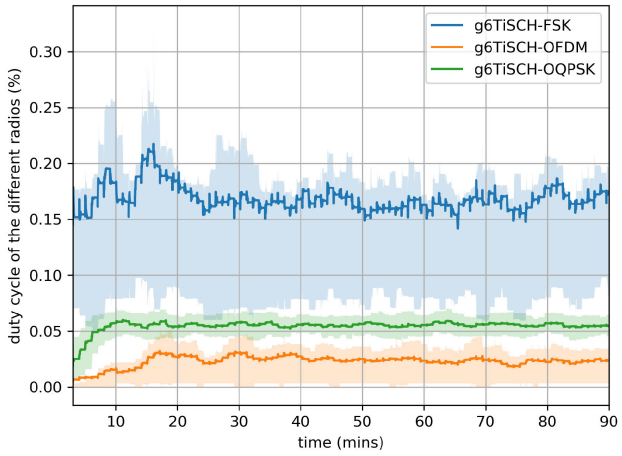

FIGURE 14. Over time, the objective function favors the use of OFDM 868 MHz over FSK 868 MHz and O-QPSK 2.4 GHz, saving on the transmission radio duty cycle.

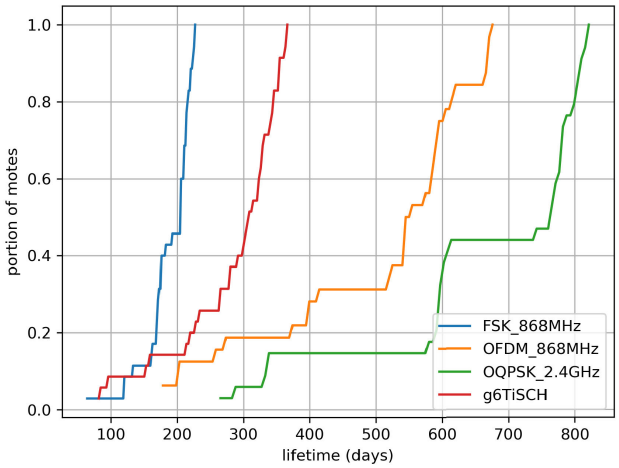

FIGURE 15. Cumulative distribution function of battery lifetime in the network demonstrates the g6TiSCH improving the energy footprint of the network compared to a pure long range FSK 868 MHz network.

It is interesting to see the benefit g6TiSCH brings to RPL as it dynamically switches to parents with faster bit rates when possible (Section IV-C). This is measured by looking at how the duty cycle of each PHY evolves over time inside the g6TiSCH network. The impact can be seen in Fig. 14 as we observe that the duty cycles of FSK 868 MHz keep decreasing over time, along with a slight increase in OFDM 868 MHz duty cycle. This is because the g6TiSCh objective function (Eq. 4) switches to parents with faster bit rates as the topology converges (based on the $Factor(PHY_i)$ parameter).

The battery lifetime of the single-PHY networks is estimated based on the power consumption of each PHY. We assume two 4.1 Wh "ideal batteries" in series, acting as a perfect voltage source (as previously assumed in [17]). Since we are only interested in the overall orders of magnitude of power consumption for each PHY, this simple battery model is sufficient for this purpose. For a given T_{TX} and T_{on} for a specific PHY, we use Eq. 6 to compute the duty cycle of transmission DC_{TX} and the duty cycle in receive mode DC_{RX}.

From the data series of the DC measurements, we compute the global DC for the steady state (last 60 mn in the network). Fig. 15 shows the expected battery lifetime at steady state for g6TiSCH compared to each single-PHY network. FSK 868 MHz has the shortest lifetime (compared to O-QPSK 2.4 GHz and OFDM 868 MHz), which was expected as it has the lowest bit-rate.

$$\begin{cases} T_{RX} = T_{on} - T_{TX} \\ DC_{TX} = \dfrac{T_{TX}}{T_{total}} \\ DC_{RX} = \dfrac{T_{RX}}{T_{total}} \end{cases} \tag{6}$$

The battery-lifetime of g6TiSCH is estimated based on the duty cycle breakdown between the three PHYs. It demonstrates generally better lifetime than the FSK 868 MHz network thanks to the overall lower duty cycle. There is an interesting room for improvement on this aspect by exploring the use of less EBs and DIOs or by reducing the maximum re-transmission attempts.

VII. CONCLUSION

This article presents g6TiSCH, a generalized 6TiSCH architecture for multi-PHY wireless networking. g6TiSCH adds agility to the protocol stack: nodes can use diverse physical layers within the same network and adapt their links depending on their conditions, while maintaining wire-like reliability.

To introduce this agility, we augment the 6TiSCH protocol stack in different ways. At the MAC layer, we add the physical layer to use for each timeslot. At the 6LoWPAN adaptation layer, we demonstrate a generalized neighbor discovery mechanism where motes discover the network over different PHYs. At the RPL layer, we adapt the routing objective function with weighted link costs.

The resulting architecture is evaluated experimentally on a testbed of 36 motes deployed in an office building. We extract KPIs important for industrial applications. Experiments with g6TiSCH show fastest network formation, lowest latency, wire-like end-to-end reliability, and improved energy footprint compared to a pure long-range network. Furthermore, our proposed objective function for IPv6 RPL successfully steers the network topology, over time, towards energy efficiency. This is achieved by dynamically switching to faster bit-rates when possible, while maintaining latency and reliability performance.

While the quantitative results are specific to this experiment, the key findings hold. First, g6TiSCH provides more controls that help achieving a more balanced performance than single-PHY networks. Second, by combining long-range and short-range radios, g6TiSCH yields lower latency and network formation time than any of the individual PHYs, while maintaining a similar battery lifetime. Third, the routing layer in g6TiSCH improves the network's energy footprint over time by selecting faster links for routing. This balances performance and energy consumption of the

network for deployments where there are both long and short distances between nodes. This provides an incentive to explore how to harness the powers of all PHYs and drive the network to create trade-offs between energy consumption and performance in diverse use-cases instead of having to choose one PHY over the other ones.

We are currently working on extending g6TiSCH with the use of slots with variable duration in the same slot frame in order to further lower latency. This way, a faster PHY can use a slot with smaller duration. This enables the network to have more compact schedule with both long and short duration slots. Furthermore, we are exploring, using RPL simulations, how to improve the battery lifetime and overall network cost of g6TiSCH. The RPL objective function can rely on different metrics to improve not just the battery lifetime, but also the financial cost, time-on-air, and link quality in the network as recently proposed in [39].

Future work includes exploring further benefits from the g6TiSCH agile multi-PHY architecture for the quality of service in industrial wireless networks. First, this architecture can allow network operators to deploy the network only once for the customer. If the customer requirements change to demand for a different mix of IEEE 802.15.4g PHYs, the network provider can just re-configure the same deployment to use a new set of PHYs. For instance, a network can initially be deployed in a relatively small area where it can sufficiently run in the 2.4 GHz band. If the customer expands their site or if they decided to require a service with lower latency, the network can be re-configured to include one or more PHYs in the sub-GHz band for more robust coverage. Second, using multi-band support, a network can make use of white-spaces in the spectrum to improve its performance (e.g. agile spectrum access) or to combat external interference in the different bands. This way, a network that is initially deployed can be re-configured to use different bands and modulations in case existing band resources become insufficient for the application. Third, the same network can be enabled to accommodate diverse applications with diverse classes of service. For instance, packets from an application with low reliability requirement and high traffic rate can be routed over faster PHYs and packets from an application with high reliability requirement and low traffic rate can be routed over slower PHYs.

REFERENCES

[1] J. Muñoz, T. Chang, X. Vilajosana, and T. Watteyne, "Evaluation of IEEE802.15.4g for environmental observations," *MDPI Sensors*, vol. 18, p. 3468, Oct. 2018.

[2] J. Munoz, E. Riou, X. Vilajosana, P. Muhlethaler, and T. Watteyne, "Overview of IEEE802.15.4g OFDM and its applicability to smart building applications," in *Proc. Wireless Days (WD)*, Dubai, UAE, Apr. 2018, pp. 123–130.

[3] A. H. Kazmi, M. J. O'grady, D. T. Delaney, A. G. Ruzzelli, and G. M. P. O'hare, "A review of wireless-sensor-network-enabled building energy management systems," *ACM Trans. Sensor Netw.*, vol. 10, no. 4, pp. 1–43, Jun. 2014.

[4] T. Watteyne, A. L. Diedrichs, K. Brun-Laguna, J. E. Chaar, D. Dujovne, J. C. Taffernaberry, and G. Mercado, "PEACH: Predicting frost events in peach orchards using IoT technology," *EAI Endorsed Trans. Internet Things*, vol. 2, no. 5, Dec. 2016, Art. no. 151711.

[5] C.-S. Sum, M.-T. Zhou, F. Kojima, and H. Harada, "Experimental performance evaluation of multihop IEEE 802.15.4/4g/4e smart utility networks in outdoor environment," *Wireless Commun. Mobile Comput.*, vol. 2017, pp. 1–13, Jan. 2017.

[6] Y. Tanaka, H. Le, V. Kobayashi, C. Lopez, T. Watteyne, and M. Rady, "Demo: Blink—Room-level localization using SmartMesh IP," in *Proc. Int. Conf. Embedded Wireless Syst. Netw. (EWSN)*, Lyon, France, Feb. 2020, pp. 198–199.

[7] T. Chang, T. Watteyne, B. Wheeler, F. Maksimovic, O. Khan, S. Mesri, L. Lee, I. Suciu, D. Burnett, X. Vilajosana, and K. Pister, "6TiSCH on SCμM: Running a synchronized protocol stack without crystals," *Sensors*, vol. 20, no. 7, p. 1912, Mar. 2020.

[8] E. Fadel, V. C. Gungor, L. Nassef, N. Akkari, M. G. A. Malik, S. Almasri, and I. F. Akyildiz, "A survey on wireless sensor networks for smart grid," *Comput. Commun.*, vol. 71, pp. 22–33, Nov. 2015.

[9] F. Civerchia, S. Bocchino, C. Salvadori, E. Rossi, L. Maggiani, and M. Petracca, "Industrial Internet of Things monitoring solution for advanced predictive maintenance applications," *J. Ind. Inf. Integr.*, vol. 7, pp. 4–12, Sep. 2017.

[10] J. Muñoz, "Km-scale industrial networking," Ph.D. dissertation, EDITE, Sorbonne Univ., Paris, France, 2019.

[11] *Datasheet: CC2538 PowerfulWireless Microcontroller System-on-Chip for 2.4-GHz IEEE 802.15.4, 6LoWPAN, and ZigBee Applications*, Texas Instrum., Dallas, TX, USA, 2015.

[12] *Nrf52840 Product Specification*, Nordic Semicond., Trondheim, Norway, 2019.

[13] *IEEE Standard for Local and Metropolitan Area Networks—Part 15.4: Low-Rate Wireless Personal Area Networks (LR-WPANs) Amendment 3: Physical Layer (PHY) Specifications for low-Data-Rate, Wireless, Smart Metering Utility Networks*, Standard IEEE 802.15.4g, Apr. 2012.

[14] *Atmel AT86RF215 Device Family Datasheet*, Atmel, San Jose, CA, USA, 2016.

[15] C. Sum, L. Lu, M. Zhou, F. Kojima, and H. Harada, "System evaluation of a practical IEEE 802.15. 4/4e/4g multi-physical and multi-hop smart utility network," *IET Commun.*, vol. 9, no. 5, pp. 665–673, Mar. 2015.

[16] T. Watteyne, X. Vilajosana, B. Kerkez, F. Chraim, K. Weekly, Q. Wang, S. Glaser, and K. Pister, "OpenWSN: A standards-based low-power wireless development environment," *Trans. Emerg. Telecommun. Technol.*, vol. 23, no. 5, pp. 480–493, Aug. 2012.

[17] M. Rady, Q. Lampin, D. Barthel, and T. Watteyne, "No free lunch—Characterizing the performance of 6TiSCH when using different physical layers," *MDPI Sensors*, vol. 20, p. 4989, Sep. 2020.

[18] M. Vucinic, T. Chang, B. Skrbic, E. Kocan, M. Pejanovic-Djurisic, and T. Watteyne, "Key performance indicators of the reference 6TiSCH implementation in Internet-of-Things scenarios," *IEEE Access*, vol. 8, pp. 79147–79157, 2020.

[19] M. Brachmann, S. Duquennoy, N. Tsiftes, and T. Voigt, "IEEE 802.15.4 TSCH in sub-GHz: Design considerations and multi-band support," in *Proc. IEEE 44th Conf. Local Comput. Netw. (LCN)*, Osnabrueck, Germany, Oct. 2019, pp. 2169–3536.

[20] D. Van Leemput, J. Bauwens, R. Elsas, J. Hoebeke, W. Joseph, and E. De Poorter, "Adaptive multi-PHY IEEE802.15.4 TSCH in sub-GHz industrial wireless networks," *Ad Hoc Netw.*, vol. 111, Feb. 2021, Art. no. 102330.

[21] C. Garrido-Hidalgo, D. Hortelano, L. Roda-Sanchez, T. Olivares, C. Ruiz, and V. Lopez, "IoT heterogeneous mesh network deployment for human-in-the-loop challenges towards a social and sustainable Industry 4.0," *IEEE Access*, vol. 6, pp. 2169–3536, May 2018.

[22] F. Lemercier, N. Montavont, L. Toutain, K. Vijayasankar, R. Vedantham, and P. Chiummiento, "Support for hybrid network in RPL," in *Proc. IEEE Int. Conf. Smart Grid Commun. (SmartGridComm)*, Sydney, NSW, Australia, Nov. 2016, pp. 527–532.

[23] A. Al-Saadi, R. Setchi, Y. Hicks, and S. M. Allen, "Routing protocol for heterogeneous wireless mesh networks," *IEEE Trans. Veh. Technol.*, vol. 65, no. 12, pp. 9773–9786, Dec. 2016.

[24] J. Muñoz, X. Vilajosana, and T. Chang, "Problem statement for generalizing 6TiSCH to multiple PHYs," IETF, Fremont, CA, USA, Tech. Rep. draft-munoz-6tisch-multi-phy-nodes-00, Jul. 2018. [Online]. Available: https://datatracker.ietf.org/doc/html/draft-munoz-6tisch-multi-phy-nodes-00 and https://datatracker.ietf.org/doc/draft-munoz-6tisch-multi-phy-nodes/00/bibtex/

[25] A. Kim, J. Han, T. Yu, and D. S. Kim, "Hybrid wireless sensor network for building energy management systems based on the 2.4 GHz and 400 MHz bands," *Inf. Syst.*, vol. 48, pp. 320–326, Mar. 2015.

[26] X. Vilajosana, T. Watteyne, T. Chang, M. Vucinic, S. Duquennoy, and P. Thubert, "IETF 6TiSCH: A tutorial," *IEEE Commun. Surveys Tuts.*, vol. 22, no. 1, pp. 595–615, 1st Quart., 2020.

[27] D. Dujovne, T. Watteyne, X. Vilajosana, and P. Thubert, "6TiSCH: Deterministic IP-enabled industrial Internet (of Things)," *IEEE Commun. Mag.*, vol. 52, no. 12, pp. 36–41, Dec. 2014.
[28] X. Vilajosana, K. Pister, and T. Watteyne, "RFC 8180: Minimal IPv6 over the TSCH mode of IEEE 802.15.4e (6TiSCH) configuration," IETF, Fremont, CA, USA, Tech. Rep. 8180, May 2017. [Online]. Available: https://datatracker.ietf.org/doc/rfc8180/bibtex/
[29] *IEEE Standard for Local and Metropolitan Area Networks—Part 15.4: Low-Rate Wireless Personal Area Networks (LR-WPANs) Amendment 1: MAC sublayer*, Standard 802.15.4e-2012, IEEE, Apr. 2012.
[30] T. Winter, P. Thubert, A. Brandt, J. Hui, R. Kelsey, P. Levis, K. Pister, R. Struik, J. Vasseur, and R. Alexander, "RFC 6550: RPL: IPv6 routing protocol for low-power and lossy networks," IETF, Fremont, CA, USA, Tech. Rep. 6550, Mar. 2012. [Online]. Available: https://datatracker.ietf.org/doc/rfc6550/bibtex/
[31] J. Vasseur, M. Kim, K. Pister, N. Dejean, and D. Barthel, "RFC 6551: Routing metrics used for path calculation in low-power and lossy networks," IETF, Fremont, CA, USA, Tech. Rep. 6551, Mar. 2012. [Online]. Available: https://datatracker.ietf.org/doc/rfc6551/bibtex/
[32] P. Thubert, "RFC 6552: Objective function zero for the routing protocol for low-power and lossy networks (RPL)," IETF, Fremont, CA, USA, Tech. Rep. 6552, Mar. 2012. [Online]. Available: https://datatracker.ietf.org/doc/rfc6552/bibtex/
[33] Q. Wang, X. Vilajosana, and T. Watteyne, "RFC 8480: 6TiSCH operation sublayer (6top) protocol (6P)," IETF, Fremont, CA, USA, Tech. Rep. 8480, Nov. 2018. [Online]. Available: https://datatracker.ietf.org/doc/rfc8480/bibtex/
[34] T. Chang, M. Vucinic, X. Vilajosana, S. Duquennoy, and D. Dujovne, "6TiSCH minimal scheduling function (MSF)," IETF, Fremont, CA, USA, Tech. Rep. 9033, Apr. 2020. [Online]. Available: https://datatracker.ietf.org/doc/rfc9033/bibtex/
[35] *IEEE Standard for Local and Metropolitan Area Networks—Part 15.4: Low-Rate Wireless Personal Area Networks (LR-WPANs)*, Standard IEEE 802.15.4, 2016.
[36] M. Vucinic, J. Simon, K. Pister, and M. Richardson, "Constrained join protocol (CoJP) for 6TiSCH," Tech. Rep., Jun. 2020.
[37] J. Munoz, F. Rincon, T. Chang, X. Vilajosana, B. Vermeulen, T. Walcarius, W. van de Meerssche, and T. Watteyne, "OpenTestBed: Poor Man's IoT testbed," in *Proc. IEEE Conf. Comput. Commun. Workshops (INFOCOM WKSHPS)*, Paris, France, Apr. 2019, pp. 467–471.
[38] P. Tuset, X. Vilajosana, and T. Watteyne, "OpenMote+: A range-agile multi-radio mote," in *Proc. Int. Conf. Embedded Wireless Syst. Netw. (EWSN)*, 2016, pp. 333–334.
[39] M. Rady, J.-P. Georges, and F. Lepage, "Can energy optimization lead to economic and environmental waste in LPWAN architectures?" *ETRI J.*, vol. 43, no. 2, pp. 1–14, Sep. 2020.

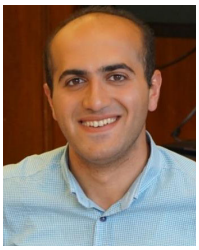

MINA RADY received the B.Sc. degree in computer science from The American University in Cairo, Egypt, in 2011, the M.Sc. degree in complex systems engineering, Université de Lorraine, France, in 2018, the M.Sc. degree in computer science from the Lappeenranta University of Technology, Finland, in 2018, and the M.Sc. degree in pervasive computing from Luleå Technical University, Sweden, in 2018. He is currently pursuing the Ph.D. degree with the EVA Laboratory, Inria, Paris, and Sorbonne University.

He was a Research Intern with the Center for Research in Automatic Control in Nancy (CRAN), France, with Professor Francis Lepage and Professor Jean-Philippe Georges on economic optimizations of LPWAN architectures. He was a Visiting Student with the Department of Political Science, Massachusetts Institute of Technology, Cambridge, MA, USA, with Professor Nazli Choucri, where he worked in the area of cyber-politics. He also worked with Dr. S. A. R. Zaidi at the Department of Electronic and Electrical Engineering, Leeds University, U.K., in the area of LPWAN topology optimization in complex terrain. He is currently a Research Engineer with Orange Labs, Meylan, France. He works in the area of heterogeneous-radio mesh networks for industrial applications.

QUENTIN LAMPIN received the degree in engineering in telecommunication systems and the Ph.D. degree in computer sciences from the National Institute of Applied Science (INSA) Lyon, in 2009 and 2014, respectively. He holds a full-time Researcher position with Orange and is a member of the Orange Expert Community. His research interest includes connectivity technologies for the IoT use cases and protocols.

DOMINIQUE BARTHEL received the degree in engineering from the Ecole Polytechnique, France, in 1985, and the degree in engineering from the SUPELEC, France, in 1987. He currently works with Orange Labs, Meylan, as a Designated Orange Expert on networks of the future. He has been researching architecture and protocols for the IoT networks, since 2000. He actively contributes to standardization of protocols for the IoT at the IETF and LoRa Alliance. The first part of his career has been devoted to architecting and designing microprocessors, and CPUs for supercomputers and real-time video processors, before moving to telecommunication and networking. He is the co-inventor of 20 international patents. He is a Senior Member of the SEE. He is the Co-Chair of the IETF ROLL Working Group, which standardizes routing in the IoT meshed networks.

THOMAS WATTEYNE (Senior Member, IEEE) received the M.Sc. degree in networking, the M.Eng. degree in telecommunications, and the Ph.D. degree in computer science from the INSA Lyon, France, in 2005, 2005, and 2008, respectively. From 2005 to 2008, he was a Research Engineer with Orange Labs (France Telecom). He was a Postdoctoral Research Lead with the Team of Prof. Kristofer Pister, University of California at Berkeley, Berkeley. He holds an Research Director position with the EVA Research Team, Inria, Paris, where he leads a team that designs, models, and builds networking solutions based on a variety of the Internet of Things (IoT) standards. He is currently a Senior Networking Design Engineer with the Dust Networks Product Group, Analog Devices, and the undisputed leader in supplying low power wireless mesh networks for demanding industrial process automation applications. He is an insatiable enthusiast of low-power wireless mesh technologies. He is fluent in four languages. He founded and co-leads Berkeley's OpenWSN Project, an open-source initiative to promote the use of fully standards-based protocol stacks for the IoT. He is a member of the IETF Internet of Things Directorate. Since 2013, he has been the Co-Chair of the IETF 6TiSCH Working Group, which standardizes how to use IEEE802.15.4e TSCH in IPv6-enabled mesh networks (http://www.thomaswatteyne.com/).